Fourier Transform Rheology of Dilute Immiscible Polymer Blends: A Novel Procedure To Probe Blend Morphology

Claudia Carotenuto,[†] Massimiliano Grosso,*[,‡] and Pier Luca Maffettone[†]

Dipartimento di Ingegneria Chimica, Università degli Studi di Napoli Federico II, Piazzale V. Tecchio 80, I-80125 Napoli, Italy, and Dipartimento di Ingegneria Chimica e Materiali, Università degli Studi di Cagliari, Piazza d'Armi, I-09123, Cagliari, Italy

Received March 10, 2008

ABSTRACT: Morphological characterization of polymer blends is important for tailoring final properties of plastic products based on these systems. A novel technique to estimate the characteristic dimension and size distribution of a polymer blend is proposed and tested. The procedure is based on Fourier transform rheology (FTR) and large-amplitude oscillatory shear experiments and exploits their sensitivity to microstructural properties. The inference protocol requires that the experimental data are analyzed with a model capable of describing the blend dynamics. This novel technique is applicable to immiscible polymer blends of practical industrial interest. The procedure is successfully tested on a model system (an immiscible polymer blend of PDMS in PIB) by treating the polymer blends with the Maffettone–Minale model coupled with the Batchelor theory.

Introduction

The technological importance of polymer blends resides in the possibility that blending two or more polymers offers to tailor the properties of a "composite" polymeric material without resorting to new specific monomers. Indeed, polymer blends represent a large and growing fraction of all plastics produced. The key points in the achievement of final products with desired properties (i.e., mechanical properties) are the features of the constituents together with the morphology or microstructure of the blend. In this work, we address the problem of characterizing such microstructure for the case of dilute immiscible polymer blends.

The typical microstructure of a dilute immiscible polymer blend at rest consists of spherical droplets immersed in a continuous matrix. The size and size distribution of these globular domains strongly affect both the processing and the mechanical properties of final products. Processing in the melt state is, of course, influenced by the peculiar rheology of this complex system and in turn influences the rheology itself by inducing microstructural changes to the blend. Indeed, strong flow conditions determine the deformation of the droplets, their possible breakup, or coalescence. Hence, the properties of the final product can be tailored by inducing during processing a designed microstructure.

The importance of inference on the morphology of the polymer blends is thus evident, as, for example, the knowledge of the characteristic average size of the droplets. This step is often performed with shearing flow experiments. Typically, either dynamic small-amplitude oscillatory shear (SAOS) flows or steady shear flows are adopted. This topic has been recently reviewed by Yu et al.,[1] who compared different methodologies to assess their efficiency in estimating blend morphology. The authors conclude that the most reliable strategy for characteristic size estimation through rheological measurements is that based on SAOS experiments. Indeed, dynamic moduli, G' and G'', can be correlated to the blend morphology through the Palierne model,[2] which is recognized as a solid theoretical tool to estimate a characteristic dimension (the volume-average radius in the case of globular morphology) of the dispersed phase. Other approaches also reveal to be efficient.[3–6]

The Palierne method gives a consistent estimation of the volume-average radius $\langle R\rangle_V$, but generally does not provide a more detailed description of the blend morphology such as, for example, a measure of sample polydispersity. In fact, G' and G'' measurements are demonstrated to be sensitive to the volume-average drop radius of the dispersed phase in the polymer blend, but they are only slightly influenced by the drop distribution at constant volume-average radius.[7] Consequently, different microstructures, characterized by the same average radius, are in general not discriminated when analyzed with SAOS experiments. To our knowledge, the distribution inference for a polymer blend based on the Palierne method has been carried out only by Friedrich et al.[8] The methodology proposed there is based on a Tikhonov regularization and gave satisfactory results only for very dilute blends with unimodal drop radius distributions.

In this paper, we propose a new experimental and inference technique to evaluate not only the characteristic dimension of the polymer blend but also the size distribution of the drops. As already mentioned, the knowledge of this distribution can be of value in the determination of the properties of the blend. The technique is based on the so-called Fourier transform rheology (FTR) which relies on large-amplitude oscillatory shear (LAOS) data. The procedure is tested here on a model system, a dilute immiscible polymer blend composed by poly(dimethylsiloxane) (PDMS) in poly(isobutylene) (PIB), but its application is completely general.

Three different batches are prepared following the same preparation protocol. Sample morphologies are preliminary characterized by means of traditional SAOS measurements. Then, LAOS experiences are carried out, and the nonlinear response is analyzed to assess its possible sensitivity to blend morphology. The experimental results obtained via LAOS measurements are then compared with theoretical predictions based on a simple ellipsoidal model for the disperse phase. In view of the good agreement found between experimental results and theoretical predictions, a new technique to extract detailed information on the blend morphology from the experimental data is finally devised.

Experimental Section and Methodologies

Materials and Sample Preparation. The polymer blend is prepared with PDMS supplied by Rhone-Poulenc (Rhodorsil

* Corresponding author. Telephone: +39 070 6755075. Fax: +39 070 6755067. E-mail: grosso@dicm.unica.it.
[†] Università degli Studi di Napoli Federico II.
[‡] Università degli Studi di Cagliari.

10.1021/ma800540n CCC: $40.75
Published on Web 05/22/2008

Table 1. Main Physical Properties of PDMS/PIB System

polymer	formula	mol wt (Da)	density (kg/m^3)	viscosity (Pa·s)	glass transition temp (°C)	interfacial tension (mN/m)
PDMS	$[-Si(CH_3)_2O-]_n$	200000	971	175	−123	3
PIB	$[-CH_2C(CH_3)_2-]_n$	1300	894	57	−70	

47V200000) and PIB purchased from Exxon (Parapol 1300). PIB and PDMS are immiscible; they are very stable and transparent at room temperature. Furthermore, they possess a relatively high viscosity and some degree of elasticity, which make them similar to industrial thermoplastic blends. For all these reasons, PIB/PDMS blend was considered a model system and was largely studied in the literature by means of both rheological and optical techniques.[4,9–12]

All the experiments were performed at constant temperature $T = 30$ °C. The main physical properties of the polymers are reported in Table 1. The value of the interfacial tension for the very same polymers is found in the literature.[13] The molecular weights are provided by the manufacturers.

Figure 1 shows the viscosity of both the pure polymers as a function of shear rate, $\dot{\gamma}$. PIB shows a constant viscosity in the investigated shear rate range, while PDMS shows just a hint of shear-thinning behavior from $\dot{\gamma} = 1$ s^{-1}. Figure 2 shows the linear dynamic viscoelasticity of the pure polymers. As expected, both the liquids possess a viscous modulus larger than the elastic one. PIB elasticity is indeed negligible, whereas, as is well-known, PDMS shows a slight elasticity.

The investigated blend has PIB as the continuous phase and PDMS as the dispersed phase. The viscosity ratio, i.e., the ratio λ between the viscosity of the dispersed phase and the continuous one, is about 3, and it is large enough to avoid significant breakup phenomena under simple shear flow.[14] Buoyancy effects are negligible in view of the similar values of the polymer densities and their high viscosities. All the experiments were carried out with a volumetric fraction, ϕ, of the dispersed phase fixed to 0.1, thus leading to a globular morphology. This value is small enough to consider coalescence negligible. Thus, the blend can be assumed to be stable, and its microstructure should not significantly vary in time during the experiments (negligible breakup and negligible coalescence).

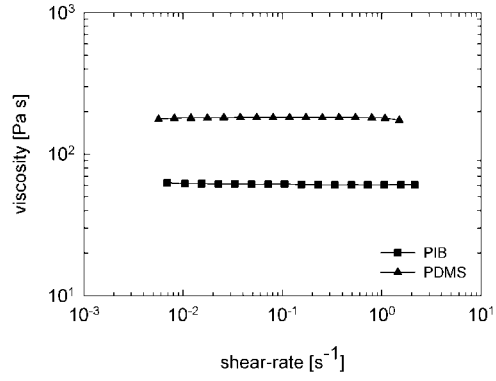

Figure 1. Viscosity versus shear rate for PIB and PDMS at 30 °C.

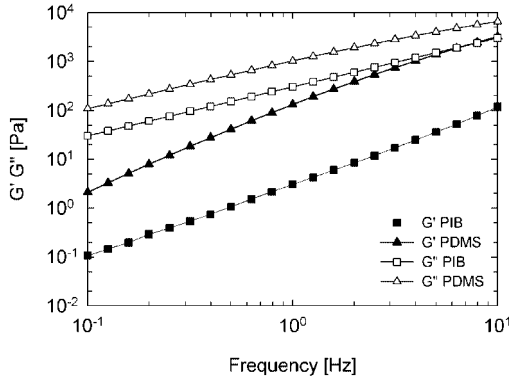

Figure 2. Elastic and viscous modulus as a function of frequency for the pure components. The temperature is 30 °C. The strain amplitude is 50%.

Samples were prepared by hand mixing the desired amounts of the two polymers in a beaker until a homogeneous white cream is obtained. Air entrained during stirring was then removed by leaving the blend under vacuum for at least one day. The very same manual preparation was already adopted by Grizzuti and Bifulco[15] who measured an average drop size of about 1−10 μm. The rheological experiments were carried out on samples which were not subjected to any pretreatment or particular flow history.

Experimental Setup. Oscillatory shear measurements (both SAOS and LAOS) were performed in a conventional strain-controlled rheometer (ARES, TA Instruments). Linear viscoelastic measurements were analyzed using the software provided by the rheometer manufacturer. LAOS experiments required a modification and improvement of the traditional rheometer data acquisition system. The raw data coming from both motor and torque transducer were acquired and digitized with a 16-bit analog to digital converter (National Instrument, PCI_6251). The motor signal was correlated to the imposed strain deformation, γ, while the torque transducer signal was associated with the measured stress. A home-written LabView routine to acquire and elaborate data was developed. Wilhelm et al.[16] pointed out that a crucial point of this kind of experimental apparatus for Fourier transform rheology is the improvement of signal-to-noise ratio (S/N). In order to maximize S/N, the rheometer was equipped with a very sensitive torque transducer (2KFRTN1) that could detect a torque ranging from 0.002 to 200 mN·m. In addition, the largest cone and plate fixture available from the TA Instrument (with a diameter of 50 mm and cone angle $\alpha = 0.02$ rad) was used to increase as much as possible the contact surface between sample and geometry and, consequently, the torque signal. In order to minimize external electronic interference, the electrical connections were double shield BNC cables (RG 223/U by Pomona). All these precautions lead to a signal-to-noise ratio higher than 10^4. It should be finally remarked that electric disturbances due to the circuitry of the rheometer itself could not be avoided. Such electric noises are not random but located at specific frequencies (50 Hz in Europe), and thus they can be easily recognized and filtered out.

Data Acquisition System. Before starting the acquisition, two main parameters were set: the scan rate, r (pts/s), and the number of data points, N_p. They were the same for both the channels (motor signal and torque signal). The ratio between N_p and r gives the time required for the entire acquisition, $t_{acq} = N_p/r$. The oscillation cycles collected during t_{acq} depend on the imposed deformation frequency (Ω_1). Typical values of r and N_p are 1×10^3 and 8×10^4 pts, respectively, thus $t_{acq} = 80$ s. Thus, for an imposed deformation frequency $\Omega_1 = 0.1$ Hz, 8 complete cycles were acquired. It should be noted that the higher values of r and N_p, the higher the S/N ratio is,[17,18] but larger t_{acq} implies larger data sets. So, the values of r and N_p were chosen to balance these two opposite factors. Furthermore, acquisitions with larger amount of data ($r = 5 \times 10^3$ pts/s and $N_p = 4 \times 10^5$ pts) have led to the very same results. Thus, one can conclude that the accuracy of data saturates with $N_p = 8 \times 10^4$ points.

Raw data coming from both motor and torque transducer were collected and subsequently transformed into the corresponding Fourier spectra. The Fourier spectrum of motor signal can be used to assess the quality of the applied deformation. The Fourier spectrum of the transducer signal shows only the fundamental harmonic in the linear regime (SAOS), while odd multiples of the fundamental harmonic appear in the nonlinear regime (LAOS). For the polymer blend under investigation, the third and the fifth

overtones could be clearly detected in the shear stress Fourier spectrum for deformation amplitudes $\gamma_0 > 100\%$.

The electric signal measured by the torque transducer is supplied in terms of potential difference units. To this end, traditional shear stress measurements were carried out and the shear stress, $\sigma(t)$, obtained with the traditional rheological measurements was then correlated to the measured electric potential, $\Delta V(t)$, according to the linear relation:

$$\sigma(t) = K \cdot \Delta V(t) \tag{1}$$

With the chosen fixture, linear regression gave $K = 125 \pm 1$ Pa/V with a 95% confidence interval.

Fourier Transform Rheology. LAOS data were analyzed according to the FTR protocols.[18,19] The imposed sinusoidal deformation is $\gamma(t) = \gamma_0 \sin(\omega_1 t)$, where $\omega_1 = 2\pi\Omega_1 = 2\pi/T$ is the characteristic angular frequency with T the oscillation period. The stress response $\sigma(t)$ preserves the periodicity of the strain forcing, but at large strain amplitudes it can no longer be represented by a simple sinusoidal waveform. The measured shear stress signal can be expressed in the Fourier domain as

$$\sigma(t) \overset{\text{FT}}{\leftrightarrow} \bar{\sigma}(\omega) = \int_{-\infty}^{\infty} \sigma(t) e^{-j\omega t}\, dt = \sum_{\substack{k=-\infty \\ \text{odd } k}}^{k=+\infty} I_k \delta(\omega - k\omega_1) \tag{2}$$

In eq 2, $\delta(\omega - k\omega_1)$ is the Dirac delta located at $\omega = k\omega_1$ ($k \in Z$), j is the imaginary unit, and I_k is the (complex) coefficient of the kth harmonic. As the stress time series $\sigma(t)$ is real valued, the condition $I_k = I^*_{-k}$ (with * denoting the complex conjugate) holds. Since the tangential stress is an odd function of the imposed strain, only odd terms of the Fourier series could be in principle accounted for in eq 2.[19] The appearance of significant values for I_k ($k > 1$) marks the onset of nonlinearities in the stress response. When dealing with finite, discrete time sampled series, a good estimation of the I_k coefficients can be carried out by finite Fourier transform algorithms.[17] The algorithm provided by Matlab is exploited. No time windowing has been carried out for the analysis.

Experimental Results

SAOS Measurements. Linear viscoelastic measurements were carried out for a preliminary characterization of the microstructure of the samples. Frequency sweep tests were performed with frequency ranging from 0.1 to 10 Hz. Strain amplitudes up to 50% gave shear stress responses well within the linear region, as proved by strain sweep tests at 0.1, 1, and 10 Hz. Furthermore, no multiples of the fundamental harmonic were clearly detectable in the stress power spectrum for $\gamma_0 < 100\%$.

Figure 3 shows the elastic modulus G' of the pure blend

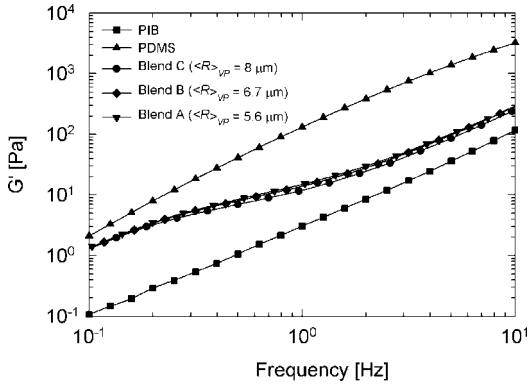

Figure 3. Elastic modulus as a function of frequency for the pure components and three different polymer blends. The brackets contain the average volumetric drop radius for each blend estimated with the Palierne model. The temperature is 30 °C. The strain amplitude is 50%.

Table 2. Relaxation Time and Average Drop Radius of Three Blends, at 30 °C

blend[a]	τ_D (s)	$\langle R\rangle_{VP}$ (μm)
A	0.53	5.6
B	0.62	6.7
C	0.70	8.0

[a] The blend composition is 10% PDMS and 90% PIB.

constituents together with those of three different blends (labeled with A, B, and C). The presence of interfaces has a very small effect on the viscous modulus and for this reason G'' is not reported in the figure. At high frequencies, the storage modulus of the blends is a weighted average of the pure components, whereas, at low frequencies, an enhanced elastic response arising from the drop interface relaxation appears. The position of the shoulder in G' and the low-frequency additional elastic contribution can be related to the blend morphology. The G' curves for the three polymer blends are almost overlapping, thus indicating that SAOS suggest that the three blends have similar morphologies. This is not surprising as the three samples under investigation were prepared following the same protocol.

Palierne[2] showed how from SAOS measurements one can obtain an estimation of the average dimension of the dispersed phase, namely the volume-average drop radius, $\langle R\rangle_V$. This scalar quantity is defined as

$$\langle R\rangle_V = \frac{\int_0^\infty R^4 \psi(R)\, dR}{\int_0^\infty R^3 \psi(R)\, dR} \tag{3}$$

where $\psi(R)$ represents the drop size distribution; i.e., $\psi(t,R)\, dR$ represents the fraction of drops that at time t have radii ranging between R and $R + dR$. Such distribution is normalized, that is, its integral over R is unity.

According to Palierne, the volume average drop radius can be easily obtained as:[7]

$$\langle R\rangle_{VP} \cong \frac{4\Gamma\tau_D}{\eta_m} \frac{10(\lambda+1) - 2\phi(5\lambda+2)}{(19\lambda+16)[2\lambda+3-2\phi(\lambda-1)]} \tag{4}$$

where Γ is the interfacial tension, η_m is the matrix viscosity, λ is the viscosity ratio of the blend, ϕ is the volumetric fraction of the dispersed phase, and τ_D is the characteristic relaxation time of the polymer blend. $\langle R\rangle_{VP}$ is the volume-average drop radius, the subscript P reminds that the value is estimated with the Palierne procedure. Equation 4 is valid for a blend constituted by two Newtonian liquids with constant interfacial tension. It gives a reasonable estimate of the volume-average drop radius for a blend with a drop distribution relatively narrow; more specifically, it is valid when the polydispersity index, PI, is smaller than 2.[7]

The polydispersity index is itself related to drop size distribution as

$$\langle R\rangle = \int_0^\infty R\psi(R)\, dR$$
$$PI = \frac{\langle R\rangle_V}{\langle R\rangle} \tag{5}$$

The polydispersity index gives a measure of the drop size dispersion: it is unity in the ideal case of a monodisperse distribution (all drops with exactly the same radius value), whereas it is greater than 1 for a polydisperse sample.

The average drop radius of the system can be obtained from eq 4 once τ_D is known. The characteristic relaxation time is identified with the relative maximum in the relaxation time spectrum of the blend. The relaxation time spectrum is here derived from the viscoelastic moduli by means of the edge preserving regularization method.[20] Table 2 contains the values of the relaxation times for the blends A, B, and C and the

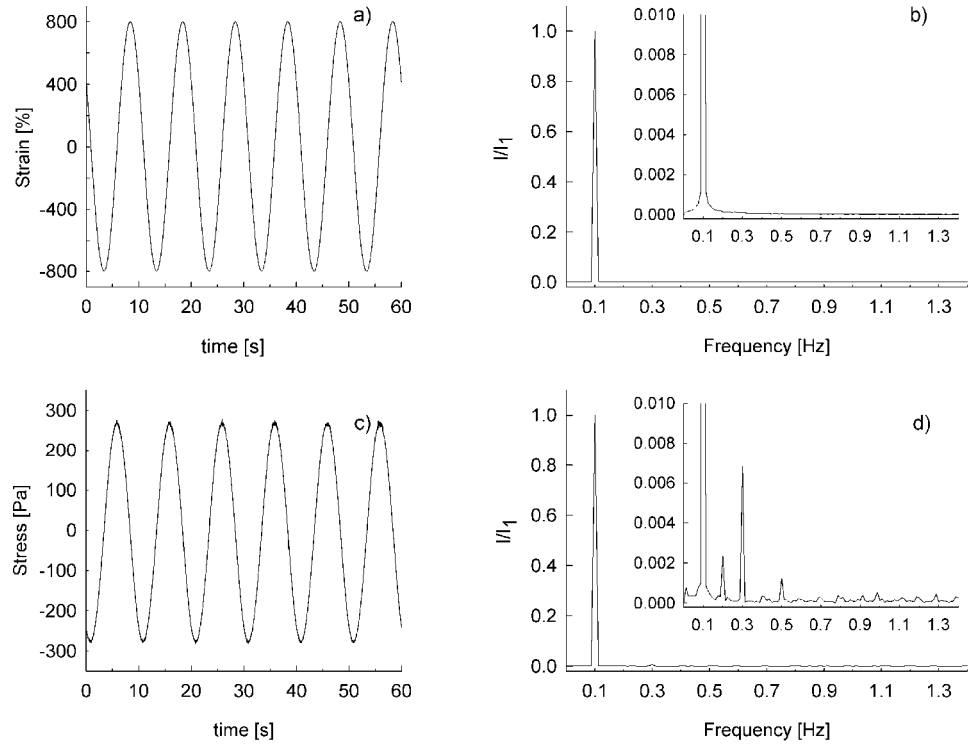

Figure 4. Motor and torque transducer signals in the time domain (a, c) and the corresponding Fourier spectra (b, d) for the polymer blend C, at 30 °C. The imposed strain deformation is 800%.

corresponding estimated average drop radii. As expected, the volume-averaged drop radius, $\langle R \rangle_{VP}$, for the three samples is very similar. These values will be used to assess the reliability of the results obtained with LAOS measurements.

LAOS Measurements. LAOS measurements were performed with $\gamma_0 \geq 200\%$. In these conditions, drop breakup can be considered negligible for the high viscosity ratio values λ. Coalescence cannot be totally excluded during the LAOS, but the small volume fraction, $\phi = 0.1$, of the dispersed phase suggests that coalescence should not be important. These considerations lead to the conclusion that the blend morphology, i.e., $\psi(R)$, can be assumed stable during LAOS experiments.

Experimental checks of the stability of blend morphology were systematically performed by means of two different methods. The first method consists of SAOS frequency sweep tests running prior, during, and after LAOS experiences. The overlapping of G' curves observed in those three stages were considered as a first indication of a constant morphology. Note, however, that this test can give only a partial confirmation of the sample stability as SAOS measurements give insights only on the volume average drop size. For this reason, every LAOS experimental procedure was repeated twice on the very same sample: the perfect overlapping of the measured nonlinear response (i.e., the overlapping of the amplitude of the higher harmonics) was considered as a further confirmation of a constant microstructure. It should be remarked that, when the experimental results did not overlap, the blend morphology was supposed to be unstable and the data were discarded.

When LAOS experiments were performed on the blends under investigation, nonlinearities in the response became clearly appreciable for $\gamma_0 \geq 200\%$. A typical experimental result is shown in Figure 4, where the applied strain and the corresponding tangential stress response are reported both in the time and in the frequency domain for $\gamma_0 = 800\%$ and $\Omega_1 = 0.1$ Hz (or, equivalently, $\omega_1 = 2\pi \times 0.1$ rad/s). The imposed deformation (Figure 4a) is a *perfect* sine wave, as confirmed by the corresponding Fourier spectrum (Figure 4b) where only the fundamental harmonic is visible. The nonlinear shear stress response cannot be easily detected in the time domain, but the corresponding power spectrum (Figure 4d) clearly shows the occurrence of a third and a fifth peak. In Figure 4d the unexpected occurrence of a second peak at twice the excitation frequency is also observable. This even harmonic can be reasonably associated to the instrument itself and results unrelated to the measured sample. For this reason it is simply neglected in this study. More detailed explanation on the occurrence of this second harmonic is reported in the Appendix. Finally, it must be noted that the Fourier spectra report the absolute value of the overtones, normalized with the first harmonic (I_k/I_1 or equivalently I_{k1}) as commonly done in the FTR literature (e.g., refs 19 and 21).

LAOS experiences were performed at different strain amplitudes, $\gamma_0 \in [200\% \div 1200\%]$. The lower limit represents the lowest deformation amplitude giving rise to a third harmonic in the shear stress clearly distinct from the background noise; the upper limit is the maximum deformation accessible without observing edge fracture. The nonlinear tests were carried out at different frequencies ranging from 0.08 to 1 Hz. Hereafter, only results obtained at frequency $\Omega_1 = 0.1$ Hz are reported. The results do not qualitatively change at different frequencies.

Figure 5 shows the ratio of the third peak of the shear stress with the fundamental one, I_{31}, as a function of the strain amplitude for the blend C. The third harmonic is clearly detected for the polymer blend under investigation. The value of I_{31} is small but reproducible with an experimental error lower than 3%. A nonmonotonic dependence on the imposed amplitude is apparent, and a clear maximum is reached at intermediate strain deformations. For the sake of comparison, data of the neat PIB and PDMS are also reported in Figure 5. The pure component I_{31} is weighted by the corresponding amount in the blend (i.e., 0.1 for the PDMS and 0.9 for the PIB). It is apparent that the I_{31} values of the pure components are extremely low, according to their quasi-Newtonian behavior, and negligible when compared with the I_{31} values of the blend. This experimental

evidence unequivocally suggests that the observed nonlinear response of the blend does not derive from simple superposition of the nonlinear contribution of the neat polymers, but it can be essentially ascribed to the interface stress contribution.

Figure 6a shows I_{31} of the three blends A, B, and C as a function of the strain amplitude. The three sets of data exhibit a similar nonmonotonic trend. However, they do not superimpose, thus suggesting that LAOS experiences could discriminate different morphologies in the polymer blends. Indeed, as reported from Palierne results, the upper curve refers to the blend A ($\langle R\rangle_{VP} = 5.6$ μm), the middle to the blend B ($\langle R\rangle_{VP} = 6.7$ μm), and the lower to the blend C ($\langle R\rangle_{VP} = 8$ μm). Hence, I_{31} of the blend increases by decreasing the mean size of the inclusions. A possible explanation of this evidence is that, at a fixed volume fraction, the specific interfacial area of the system is greater for the blend with smaller droplets thus determining an increase of the interfacial contribution. In Figure 6b, the ratio I_{51} for the blends A, B, and C is also reported. Since the fifth overtones are smaller than the third ones, they are more affected by the experimental noise. However, the three curves are clearly distinct, and they also exhibit a nonmonotonic trend. Analogously to I_{31} behavior, the fifth peaks are larger for blend with smaller volume averaged drop radius.

As already found for other systems,[22–25] also for polymer blends LAOS tests prove to be a very sensitive tool in capturing even slight differences in the material microstructure. It should be remarked that at the same frequency of data reported in Figure 6, i.e., at 0.1 Hz, the storage moduli of the blend A, B, and C substantially superimpose (see Figure 3), while I_{31} and I_{51} (see Figure 6) are clearly distinct.

Comparison with Theory

The Model Evaluated in the Fourier Domain. LAOS data are now compared with theoretical predictions. The total tensor stress $\boldsymbol{\sigma}$ of a dilute polymer blend with Newtonian constituents can be calculated according to[26]

$$\boldsymbol{\sigma} = \underbrace{-p\mathbf{I}}_{\text{isotropic term}} + \underbrace{\eta_m\left(\nabla\mathbf{v}+\nabla\mathbf{v}^{\mathrm{T}}\right)}_{\text{external contribution}} - \underbrace{\underbrace{\frac{\eta_m}{V}\int_A(\mathbf{nu}+\mathbf{un})\,dA}_{\text{viscous term}} - \underbrace{\frac{\Gamma}{V}\int_A\left(\mathbf{nn}-\frac{1}{3}\mathbf{I}\right)dA}_{\text{elastic term}}}_{\text{interfacial contribution}} \tag{6}$$

In eq 6, p is the pressure, $\nabla\mathbf{v}$ is the undisturbed velocity gradient tensor and $\nabla\mathbf{v}^{\mathrm{T}}$ its transpose, η_m is the viscosity of the continuous phase, V is the total volume of the system, $\mathbf{n}$ is the unit vector normal to the interface between the two phases, $\mathbf{u}$ is the velocity at the interface, dA is the area of an interfacial element, and the integrals are calculated over the whole interface of the system, A. Equation 6 can be used to predict the stresses if $\mathbf{n}$ and $\mathbf{u}$ are known. As in dilute conditions the typical blend morphology is globular, for a given imposed flow field those two vectors depend only on the drop radius R and may vary in time as the drop shape may vary. In dilute conditions, drop interactions can be neglected. We assume that in the LAOS experiments under investigation each drop of the population can be treated as an isolated drop in a matrix, with the LAOS flow being imposed at infinity. In the following, only the shear stress component, $\sigma(t)$, of eq 6 will be considered, and the instantaneous stress will be calculated by considering the instantaneous drop configuration.

Equation 6 is the sum of two conceptually different terms: the first one is due to the Newtonian matrix contribution and depends linearly on the velocity gradient, whereas the second term is an integral corresponding to the sum of interfacial contributions related to the entire drop population. The first part depends linearly on the applied shear rate, whereas the interfacial contribution is the only nonlinear term appearing in eq 6. Under LAOS, the first term will not contribute to higher harmonics in the shear stress for its linear nature. Conversely, the interface component will give rise to higher harmonics in the power spectrum of $\sigma(t)$.[27] Consequently, the contribution to the higher harmonics in the Fourier spectrum of each drop with radius R is directly related to the interfacial contribution. In the frequency domain this can be written as

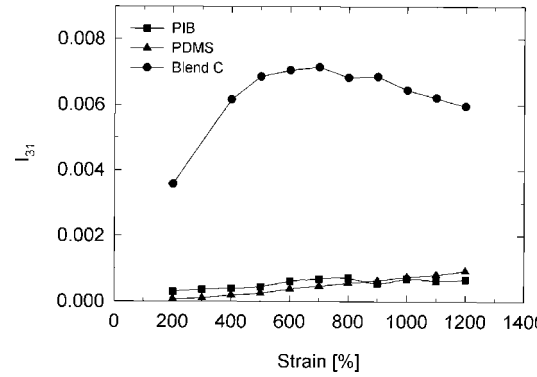

Figure 5. Absolute value of third harmonic normalized with the corresponding first harmonic as a function of the imposed strain deformation for the pure components and for the blend C. The temperature is 30 °C. The oscillation frequency is 0.1 Hz.

$$I_k(R) = \frac{2\pi}{T}\int_T \sigma(t)e^{-jk\omega t}dt = -\frac{2\pi}{T}\int_T\underbrace{\left(\frac{\eta}{V}\int_A(\mathbf{nu}+\mathbf{un})\,dA + \frac{\Gamma}{V}\int_A\left(\mathbf{nn}-\frac{1}{3}\mathbf{I}\right)dA\right)}_{\text{interfacial contribution}}e^{-jk\omega t}\,dt \tag{7}$$

with k odd and >1.

We now briefly resume the procedure proposed in ref 27 to estimate the drop size morphology in polydisperse blends through LAOS measurements. When dealing with dilute systems, the total tangential interfacial stress $\sigma(t)$ is assumed to derive from the linear superposition of the contributions pertaining each single drop. Thus, $\sigma(t)$ term depends on an integral involving the drop population:

$$\sigma(t) = \int_\Lambda \sigma_I(R,t)\psi(R)\,\mathrm{d}R \tag{8}$$

where $\sigma_I(R,t)$ is the interfacial stress contribution of eq 7 calculated for a drop of radius R, $\psi(R)$ is the unknown drop distribution to be estimated, and Λ is the domain of the $\psi(R)$ distribution. Equation 8 can be easily rephrased in the Fourier domain combining the linear nature of the Fourier transform with the linearity of the integral operator:

$$I_k = \int_\Lambda I_k(R)\psi(R)\,\mathrm{d}R, \quad k>1,\ k \text{ odd} \tag{9}$$

Within these assumptions, eq 9 states that, if the distribution function $\psi(R)$ is known a priori, the *direct* problem of estimation of the total I_k starting from the evaluations of $I_k(R)$ numerically calculated by varying the drop radius R is a linear problem. Here, we are interested in the *inverse* problem, that is, the estimation of the distribution $\psi(R)$ by means of the experimental observations I_k. Note that this inverse problem, obviously, is still linear in nature.

Of course, a point estimation of $\psi(R)$ is not possible. For this reason, we introduce a coarse-grained description $\varphi(R;\mathbf{b})$ (with $\mathbf{b} \in R^p$) which reasonably approximates the drop size distribution:

$$\psi(R) \approx \varphi(R;\mathbf{b}) = \sum_i b_i \nu_i(R) \tag{10}$$

In eq 10, the approximating function $\varphi(R;\mathbf{b})$ is a linear sum of elements belonging to a proper set of basis functions $\nu_i(R)$ ($R \in \Lambda$, i finite). The b_i terms represent the amount of each basis function contributing to the distribution, and they are, finally,

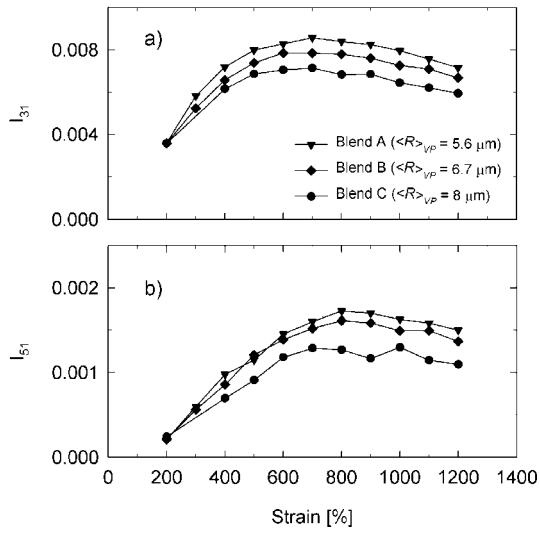

Figure 6. Absolute value of the (a) third and (b) fifth harmonic normalized with the first one as a function of strain amplitude for the blend A, B, and C. The oscillation frequency is 0.1 Hz.

the unknown coefficients to be estimated. Thus, the higher harmonics in the power spectrum can be definitely rewritten, after some simple passages, as

$$I_k \approx \int_\Lambda I_k(R)\phi(R)\,\mathrm{d}R = \int_\Lambda I_k(R)\sum_i b_i \nu_i(R)\,\mathrm{d}R = \sum_i b_i \int_\Lambda I_k(R)\nu_i(R)\,\mathrm{d}R = \sum_i b_i I_k(\nu_i) \quad (11)$$

In eq 11, k is odd and >1, and $I_k(\nu_i) = \int_\Lambda I_k(R)\nu_i(R)\,\mathrm{d}R$.

It should be noted that the term $I_k(\nu_i)$ can be a priori calculated through integration of a mathematical model describing drop deformation, once a proper set of basis functions is selected. In the end, the evaluation of the b_i terms is an inverse linear problem which can be easily solved through a multiple linear regression.

The inversion procedure needs the prior evaluation of the $I_k(\nu_i)$ terms. To this end, the interface stress can be estimated by means of eq 7 provided the instantaneous drop deformation is available. For a detailed comparison with the experimental results, one could obtain this latter information from accurate numerical simulations.[28,29] An easier comparison can be obtained, however, with phenomenological models for drop deformation. Several ellipsoidal models have been proposed to describe drop dynamics under generic flow conditions.[30–33] Here we use the model proposed by Maffettone and Minale[30] also known as the MM model.

The drop is described as an ellipsoid by a second-rank symmetric, positive definite, and time-dependent tensor **S**. The shape dynamics can be thus described by the evolution of tensor **S** which follows the nondimensional equation:

$$\frac{\partial \mathbf{S}}{\partial t} - (\mathbf{\Omega}\cdot\mathbf{S} - \mathbf{S}\cdot\Omega) = -f_1\left(\mathrm{S} - \frac{3}{II_2}\mathbf{I}\right) + f_2(\mathrm{S}\cdot\mathbf{D} + \mathbf{D}\cdot\mathrm{S}) \quad (12)$$

In eq 12, time is made nondimensional with the emulsion time ($\eta_m R/\Gamma$), where η_m is the matrix viscosity, R is the undistorted drop radius, and Γ is the interfacial tension; **I** is the second-rank unit tensor, **D** and **Ω** are the deformation rate and the vorticity tensors, respectively, and II_2 is the second scalar invariant of tensor **S**. The shear flows here considered give the following forms for the deformation and vorticity tensors:

$$D = \frac{1}{2}\mathrm{Ca}(t)\begin{pmatrix}0 & 1 & 0\\ 1 & 0 & 0\\ 0 & 0 & 0\end{pmatrix}, \quad \mathbf{\Omega} = \frac{1}{2}\mathrm{Ca}(t)\begin{pmatrix}0 & 1 & 0\\ -1 & 0 & 0\\ 0 & 0 & 0\end{pmatrix} \quad (13)$$

where Ca(t) is the time-dependent capillary number, Ca = $R\eta_m\dot{\gamma}(t)/\Gamma$. The functions f_1 and f_2 appearing in eq 12 are given by[30]

$$f_1(\lambda) = \frac{40(\lambda+1)}{(2\lambda+3)(19\lambda+16)}$$
$$f_2(\lambda,\mathrm{Ca}) = \frac{5}{2\lambda+3} + \frac{3\mathrm{Ca}^2}{2+6\mathrm{Ca}^2} \quad (14)$$

At rest the drop is spherical (**S** = **I**). Notice finally that within this description drop breakup is absent under shear flow for $\lambda \geq 3$.

The MM model was proven to give quantitative agreement with experimental results up to Ca values slightly larger than unity.[34] The largest capillary number attained during LAOS is $\mathrm{Ca}_{max} = 2\pi\omega_1\gamma_0\eta_m R_{max}/\Gamma$. The largest drop radius R_{max} was speculated as $\sim 2\langle R\rangle_{VP}$, that is $R_{max} \sim 16\ \mu$m. Thus $\mathrm{Ca}_{max} \sim 1.5$, a value which allows us to consider the MM model adequate to describe the drop dynamics.

In the following, the viscous term in the interfacial stress (eq 6) is assumed to be negligible, and the stress computations were performed by taking into account the only elastic interfacial term.

Comparison with the Model. According to eq 9, the tangential stress, $\sigma(t)$, in the Fourier domain results from the linear superposition of the contributions pertaining to each drop of the population. The coarse grained approximation $\varphi(R)$ of the drop population is carried out by exploiting boxcar functions[35] as basis functions, i.e. uniform functions equal to 1 within the range $[R_i - \Delta R/2, R_i + \Delta R/2]$ (ΔR being the thickness of the single boxcar function), and nil outside that range. Other basis functions can be also adopted (e.g., Gaussian functions). However, we refer to these basis boxcar functions since they lead to a simple evaluation of the $I_k(\nu_i)$ terms. Here, the drop population is approximated with the sum of eight basis functions, covering the range of values $\Lambda = [0, 16\ \mu\mathrm{m}]$. Thus, the number of coefficients b_i in eq 13 to be estimated by means of the multiple linear regression is $p = 8$. The choice of the size domain for the drop distribution is not a trivial point, and this aspect leads to an arbitrary selection. As already mentioned, we assume that the largest drop radius in the drop population is $R_{max} = 2\langle R\rangle_{VP} = 16\ \mu$m. The amplitude of each boxcar, ΔR, is assumed to be constant $\Delta R = 2\ \mu$m.

In order to achieve a quantitative description of the blend microstructure, the real and the imaginary part of the multiple harmonics are required.[27] They are indicated, respectively, with the symbols Re(I_k) and Im(I_k). Furthermore, these quantities are not normalized with the amplitude of the first harmonic, but with the amplitude of the imposed deformation. Consequently, $\mathrm{Re}(I_k)/\gamma_0$ and $\mathrm{Im}(I_k)/\gamma_0$ are dimensional quantities (stresses). Each LAOS experience leads to four experimental data which can be used for the distribution inference procedure. Since the number of LAOS experiments conducted for each sample was $M \sim 10$, the number of experimental points used in the regression is $N = 4M$. This number is much larger than the number of parameters, p, to be estimated, as required to achieve a statistically significant parameter inference. A constrained linear regression[36] was used here, since the regression parameters b_i are constrained to be positive. As a final remark, it should be noticed that the procedure adopted here does not need any Tikhonov regularization.[8] This is not a minor aspect, since the latter approach is a particular case of ridge regression, and it leads however to a biased parameter estimation.[37]

The goodness of fit of the model was measured by computing the mean square error, MSE, and the determination coefficient, R^2:

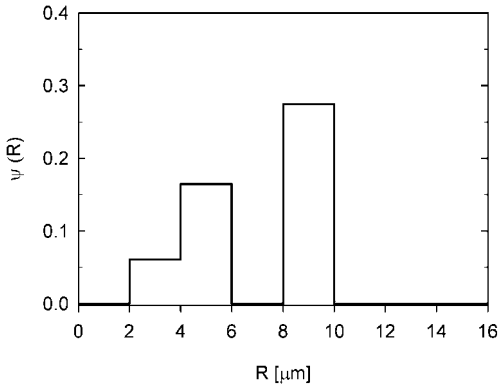

Figure 7. Drop distribution estimated with the regression procedure for the blend C.

$$\mathrm{MSE} = \frac{\sum_{k=3,5}\sum_{n=1}^{M}(\mathrm{Re}(\hat{I}_k(n)) - \mathrm{Re}(I_k(n)))^2 + \sum_{k=3,5}\sum_{n=1}^{M}(\mathrm{Im}(\hat{I}_k(n)) - \mathrm{Im}(I_k(n)))^2}{N-p} \tag{15}$$

$$R^2 = \frac{\sum_{k=3,5}\sum_{n=1}^{M}(\mathrm{Re}(\hat{I}_k(n)) - \mathrm{Re}(I_k(n)))^2 + \sum_{k=3,5}\sum_{n=1}^{M}(\mathrm{Im}(\hat{I}_k(n)) - \mathrm{Im}(I_k(n)))^2}{\sum_{k=3,5}\sum_{n=1}^{M}(\mathrm{Re}(\hat{I}_k(n)) - \bar{I}_k)^2 + \sum_{k=3,5}\sum_{n=1}^{M}(\mathrm{Im}(\hat{I}_k(n)) - \bar{I}_k)^2} \tag{16}$$

with

$$\bar{I}_k = \frac{\sum_{k=3,5}\sum_{n=1}^{M}\mathrm{Re}(I_k(n)) + \sum_{k=3,5}\sum_{n=1}^{M}\mathrm{Im}(I_k(n))}{N}$$

In eqs 15 and 16, $I_k(n)$ and $\hat{I}_k(n)$ are respectively the observed values and the theoretical predictions for the kth harmonic at the nth experiment ($n = 1, ..., M$). In eq 16, $\bar{I}_k$ is the average value of all the overtones (both real and imaginary part) in the experimental power spectrum that were used for the inference. The MSE scalar gives a measure of the distance between the observed values of the harmonics $I_k(n)$ and the corresponding theoretical predictions $\hat{I}_k(n)$ provided by the model, whereas the determination coefficient R^2 in eq 16 is the proportion of variability in the data set that is accounted for by the statistical model. The R^2 coefficient gives information about goodness of fit of the model. Usually, it assumes values between 0 and 1 and the quality of fit increases as R^2 tends to the unity.

The distribution inference also allows the evaluation of some important scalars as the number-average radius, the volume-average radius, and the polidispersity index.

For sake of brevity, we report the detail of the procedure only for the blend C, where Palierne model has given an average drop radius $\langle R\rangle_{VP} = 8.0\ \mu$m. The drop distribution estimated with the procedure is reported in Figure 7. It appears that the drop population has a bimodal nature: the 50%, circa, of the drop population shows a radius estimated between 8 and 10 μm. In addition, a not negligible amount of drops with a smaller radius (between 2 and 6 μm) is evidenced. A bimodal distribution for the very same blend in the same conditions (temperature and flow conditions) has been already observed in the literature via optical measurements.[15] Thus, LAOS measurements demonstrate to be a valuable tool to detect and quantify sample polydispersity. Incidentally, the average drop radius estimated with the actual distribution is equal to $\langle R\rangle = 7.0\ \mu$m, and the volume-average radius is $\langle R\rangle_V = 8.8\ \mu$m. These estimations are very close to the volume-average radius obtained with the Palierne method. As a final remark, it should be mentioned that the occurrence of a nonnegligible amount of drops with small radius is plausible, and this feature was also already experimentally observed,[9,15] especially when dealing with large strain deformations.[12]

In Figure 8 (circle symbols), the real and the imaginary part of the third and the fifth harmonic normalized with the strain amplitude of the blend C are reported. Panels a and b show the real and the imaginary part of the ratio I_3/γ_0, respectively, whereas panels c and d illustrate the real and imaginary part of the ratio I_5/γ_0. The experimental results (symbols) show some peculiarities both for the real and the imaginary part of the power spectrum. The theoretical predictions are plotted as lines in Figure 8 and were obtained with a fit with $\mathrm{MSE} = 4.94 \times 10^{-4}$ and $R^2 = 0.967$. The agreement between experimental data and model is remarkable, and it is quantitative for the third harmonic. Some disagreement is found when comparing theory and experiments for the fifth harmonic. However, theoretical predictions correctly capture the qualitative behavior of the fifth harmonic: the occurrence of a minimum in the $\mathrm{Re}(I_5/\gamma_0)$ curve and the decreasing nature, with a flex at intermediate deformation, of the imaginary part of the fifth harmonic. The partial discrepancy can have several motivations. First, one should notice that the higher harmonics are more sensitive to experimental noise. Another plausible reason can be the loss of efficiency of the model. Incidentally, one should note that interfacial stress in eq 9 has been calculated by neglecting the viscous contribution, and this assumption can have an impact for some experimental conditions, especially when dealing with large-amplitude oscillations.

The inference results are summarized in Table 3, which reports the MSE (column 6) and R^2 (column 7) statistics together with the main features of the estimated drop distributions: the average drop radius (column 3), the volume-average radius (column 4), and the polidispersity index PI (column 5). For sake of completeness, also the volume-average radius $\langle R\rangle_{VP}$ estimated with the Palierne procedure is reported (column 2). The current comparison between theory and experiments suggests some remarks. In all cases the discrepancy between theory and observation is small, and the determination coefficient is really close to the unity. The average radii (both linear and volumetric) are close to the estimates obtained with the Palierne methodology. Finally, with the proposed approach, a sound estimation of the polidspersity index can be reached, and this quantity is barely appreciable with the traditional SAOS protocols. It must be noted that the polidispersity index (column 5) is relatively low ($\sim$1.3) for all the blends here considered. This result justifies the validity of the predictions obtained with the simplified version of the Palierne model.[7]

Appendix: On the Occurrence of the Even Harmonics

Second harmonic and, more generally, even harmonics are not predicted by theory except for some specific case (e.g., materials with high elasticity level combined with strong inertia effect[38]). Nevertheless, even peaks in the power spectrum are often encountered in LAOS experiences.[18,19,39–41] The occurrence of a second harmonic, I_2, is also evident in the blend power spectrum here reported in Figure 4d.

Several explanations for the presence of even overtones in the spectra have been proposed in the literature. Quite often, the occurrence of even harmonics is ascribed to some defects in the experiments[42] as wall-slip phenomena.[43–45] Alternatively,

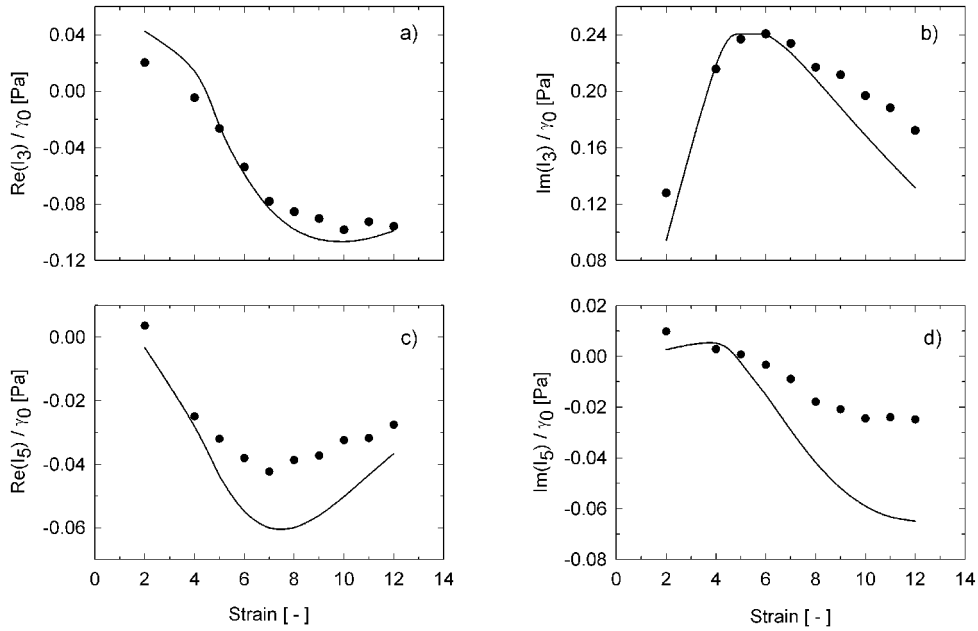

Figure 8. Real and imaginary part of the third and the fifth harmonic normalized with the strain amplitude for the blend C. The oscillation frequency is 0.1 Hz. Circle symbols refer to experimental points, solid lines refer to theoretical prediction.

Table 3. Summary of the Results Obtained for the Distribution Inference for the Three Blends[a]

blend	$\langle R\rangle_{VP}$ (μm)	$\langle R\rangle$ (μm)	$\langle R\rangle_{V}$ (μm)	PI	MSE	R^2
A	5.6	6.090	7.867	1.29	6.37×10^{-4}	0.974
B	6.7	6.272	8.058	1.28	5.36×10^{-4}	0.973
C	8.0	7.037	8.796	1.25	4.94×10^{-4}	0.967

[a] $\langle R\rangle_{VP}$ is the volume-average drop radius estimated with the Palierne procedure. $\langle R\rangle$ is the number-average drop radius estimated with FTR procedure. $\langle R\rangle_{V}$ is the volume-average drop radius estimated with FTR procedure.

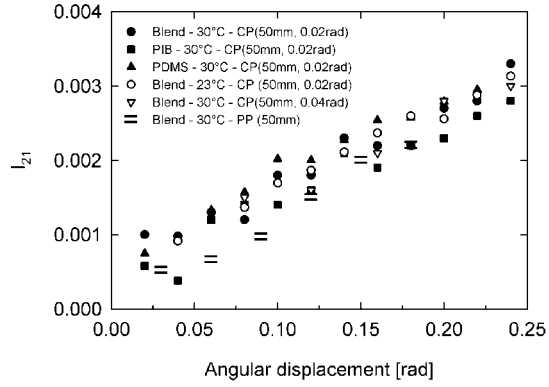

Figure 9. Normalized second harmonic as a function of the angular displacement of the oscillating plate for different systems, at two different temperatures and for three different geometries. The oscillation frequency is 0.1 Hz.

Wilhelm et al.[19] motivate the presence of even peaks as deriving from "a time-dependent memory effect or nonlinear elastic contribution in the system". It should be, however, noticed that all the explanations found in the literature are material dependent. Conversely, in our case the second harmonic seems to be material independent, and it is attributed to an imperfect alignment of the upper and lower plates of the rheometer. Figure 9 shows the second harmonic normalized with the first one, I_{21}, as a function of the angular displacement for different samples (pure PIB, pure PDMS, PDMS/PIB-10/90), at two different temperatures (23 and 30 °C) and also for three different geometries (two cone and plate and one parallel plate). It is apparent that the second peak is quite similar for all the systems at any angular displacement Θ. Furthermore, I_{21} shows a linear dependence on the angular displacement.

Final Remarks

In this work, a novel procedure based on Fourier transform rheology is proposed to estimate the morphology of a polymer blends. The polymer blend is subjected to LAOS tests, and the corresponding stress response is analyzed in the Fourier domain. The procedure is successfully tested on a model system, i.e., a dilute immiscible polymer blend with Newtonian constituents (PIB/PDMS).

The methodology exploits sensitivity of LAOS experiences to the microstructural properties of the liquids. The inference on the experimental data requires a model capable of describing the blend dynamics. To this end, here we have used the Maffettone and Minale model coupled with Batchelor theory. For data taken with the model system, good agreement is found between predictions and observations: not only can the average drop dimension be efficiently estimated with results very close to those obtained with Palierne model and SAOS experiments but also sound information on the drop size distribution can be achieved. This latter property is not easily appreciated with traditional linear spectroscopy.

We do believe that the success in describing our experimental data taken on a model system is very promising for the rather general applicability of the technique to the characterization of polymer blends of practical industrial interest. Indeed, LAOS experiments once analyzed with our technique could represent an innovative methodology to characterize the morphology (size and size distribution) of polymer blends of interest in the applications.

References and Notes

(1) Yu, W.; Bousmina, M.; Zhou, C. Note on morphology determination in emulsions via rheology. *J. Non-Newtonian Fluid. Mech.* **2006**, *133*, 57–62.
(2) Palierne, J. F. Linear rheology of viscoelastic emulsions with interfacial tension. *Rheol. Acta* **1990**, *29*, 204–214.
(3) Bousmina, M. Rheology of polymer blends: linear model for viscoelastic emulsions. *Rheol. Acta* **1999**, *38*, 73–83.
(4) Jansseune, T.; Mewis, J.; Moldenaers, P.; Minale, M.; Maffettone, P. L. Rheology and rheological morphology determination in im-

miscible two-phase polymer blends. *J. Non-Newtonian Fluid Mech.* **2000**, *93*, 153–165.
(5) Yu, W.; Bousmina, M.; Grmela, M.; Palierne, J. F.; Zhou, C. Quantitative relationship between theory and morphology in emulsions. *J. Rheol.* **2002**, *46*, 1381–1399.
(6) Minale, M.; Maffettone, P. L. Morphology estimation from normal stress measurements for dilute immiscible polymer blends. *Rheol. Acta* **2003**, *42* (1−2), 158–165.
(7) Graebling, D.; Muller, R.; Palierne, J. F. Linear viscoelastic Behavior of Some Incompatible Polymer Blends in the Melt. Interpretation of Data with a Model of Emulsion of Viscoelastic Liquids. *Macromolecules* **1993**, *26*, 320–329.
(8) Friedrich, C.; Gleinser, W.; Korat, E.; Maier, D.; Weese, J. Comparison of sphere-size distributions obtained from rheology and transmission electron microscopy in PMMA/PS blend. *J. Rheol,* **1995**, *39* (6), 1411–1425.
(9) Vinckier, I.; Moldenaers, P.; Mewis, J. Relationship between rheology and morphology of model blends in steady shear flow. *J. Rheol.* **1996**, *40* (4), 613–631.
(10) Minale, M.; Moldenaers, P.; Mewis, J. Transient flow experiments in a model immiscible polymer blend. *J. Rheol.* **1999**, *43* (3), 815–827.
(11) Guido, S.; Minale, M.; Maffettone, P. L. Drop shape dynamics under shear-flow reversal. *J. Rheol.* **2000**, *44* (6), 1385–1399.
(12) Wannaborworn, S.; Mackley, M. R.; Renardy, Y. Experimental observation and matching numerical simulation for the deformation and breakup of immiscible drops in oscillatory shear. *J. Rheol.* **2002**, *46* (5), 1279–1293.
(13) Sigillo, I.; Di Santo, L.; Guido, S.; Grizzuti, N. Comparative Measurements of Interfacial Tension in a Model Polymer Blend. *Polym. Eng. Sci.* **1997**, *37* (9), 1540–1549.
(14) Grace, H. P. Dispersion phenomena in high viscosity immiscible fluid systems and application of static mixers as dispersion devices in such systems. *Chem. Eng. Commun.* **1982**, *14*, 225–277.
(15) Grizzuti, N.; Bifulco, O. Effect of coalescence and break up on the steady-state morphology of an immiscible polymer blend in shear flow. *Rheol. Acta* **1997**, *36*, 406–415.
(16) Wilhelm, M.; Reinheimer, P.; Ortseifer, M. High sensitivity Fourier-transform rheology. *Rheol. Acta* **1999**, *38*, 349–356.
(17) Bracewell, R. N. *The Fourier-transform and its application*; McGraw-Hill: New York, 1986.
(18) Wilhelm, M. Fourier Transform Rheology. *Macromol. Mater. Eng.* **2002**, *287*, 83–105.
(19) Wilhelm, M.; Maring, D.; Spiess, H. W. Fourier Transform Rheology. *Rheol. Acta* **1998**, *37*, 399–405.
(20) Roths, T.; Maier, D.; Friedrich, C.; Marth, M.; Honerkamp, J. Determination of the relaxation time spectrum from dynamic moduli using an edge preserving regularization method. *Rheol. Acta* **2000**, *39*, 163–173.
(21) Neidhöfer, T.; Wilhelm, M.; Debbaut, B. Fourier-transform rheology experiments and finite-element simulations on linear polystyrene solutions. *J. Rheol.* **2003**, *47* (6), 1351–1371.
(22) Kallus, S.; Willenbacher, N.; Kirsch, S.; Distler, D.; Neidhöfer, T.; Wilhelm, M.; Spiess, H. W. Characterization of polymer dispersions by Fourier transform rheology. *Rheol. Acta* **2001**, *40*, 552–559.
(23) Langela, M.; Wiesner, U.; Spiess, H. W.; Wilhelm, M. Microphase Reorientation in Block Copolymer Melts as Detected via FT Rheology and 2D SAXS. *Macromolecules* **2002**, *35*, 3198–3204.
(24) Neidhöfer, T.; Siuola, S.; Hadjichristidis, N.; Wilhelm, M. Distinguish Linear from Star Branched Polystyrene Solutions with Fourier Transform Rheology. *Macromol. Rapid Commun.* **2004**, *25*, 1921–1926.
(25) Schlatter, G.; Fleury, G.; Muller, R. Fourier Transform Rheology of Branched Polyethylene: Experiments and Models for Assessing the Macromolecular Architecture. *Macromolecules* **2005**, *38*, 6492–6503.
(26) Batchelor, G. K. The stress system in a suspension of force-free particles. *J. Fluid Mech.* **1970**, *41*, 545–570.
(27) Grosso, M.; Maffettone, P. L. A new methodology for the estimation of drop size distributions of dilute polymer blends based on LAOS flows. *J. Non Newtonian Fluid Mech.* **2007**, *143*, 48–58.
(28) Cristini, V.; Blawzdziewicz, J.; Loewenberg, M. An adaptive mesh algorithm for evolving surfaces: Simulations of drop breakup and coalescence. *J. Comput. Phys.* **2001**, *168* (2), 445–463.
(29) Renardy, Y. Numerical simulation of a drop undergoing large amplitude oscillatory shear. *Rheol. Acta* **2006**, *45*, 223–227.
(30) Maffettone, P. L.; Minale, M. Equation of change for ellipsoidal drops in viscous flows. *J. Non-Newtonian Fluid Mech.* **1998**, *78*, 227–241.
(31) Bousmina, M.; Aouina, M. B.; Chaudhry, R.; Guenette, R. E. S. Bretas, Rheology of polymer blends: non-linear model for viscoelastic emulsions undergoing high deformation flows. *Rheol. Acta* **2001**, *40*, 538–551.
(32) Yu, W.; Bousmina, M. Ellipsoidal model for droplet deformation in emulsions. *J. Rheol.* **2003**, *47* (4), 1011–1039.
(33) Almusallam, A. S.; Larson, R.; Solomon, M. J. Comprehensive constitutive model for immiscible blends of Newtonian polymers. *J. Rheol.* **2004**, *48* (2), 319–348.
(34) Guido, S.; Grosso, M.; Maffettone, P. L. Newtonian drop in a Newtonian matrix subjected to large amplitude oscillatory shear flows. *Rheol. Acta* **2004**, *43*, 575–583.
(35) Weisstein, E. W. "Boxcar Function." From MathWorld--A Wolfram Web Resource. http://mathworld.wolfram.com/BoxcarFunction.html.
(36) Coleman, T. F.; Li, Y. A Reflective Newton Method for Minimizing a Quadratic Function Subject to Bounds on Some of the Variables. *SIAM J. Optimization* **1996**, *6* (4), 1040–1058.
(37) Hoerl, A. E.; Kennard, R. W. Ridge regression: biased estimation for non-orthogonal problems. *Technometrics* **1970**, *12*, 69–82.
(38) Atalik, K.; Keunings, R. On the occurrence of even harmonics in the shear stress response of viscoelastic fluids in large amplitude oscillatory shear. *J Non-Newtonian Fluid Mech.* **2004**, *122*, 107–116.
(39) Debbaut, B.; Burhin, H. Large amplitude oscillatory shear and Fourier-transform rheology for a high-density polyethylene: Experiments and numerical simulation. *J. Rheol.* **2002**, *46* (5), 1155–1176.
(40) Neidhöfer, T.; Sioula, S.; Hadjichristidis, N.; Wilhelm, M. Distinguishing Linear from Star-Branched Polystyrene Solutions with Fourier-Transform Rheology. *Macromol. Rapid Commun.* **2004**, *25*, 1921–1926.
(41) Hyun, K.; Nam, J. G.; Wilhelm, M.; Ahn, K. H.; Lee, S. J. Nonlinear response of complex fluids under LAOS (large amplitude oscillatory shear) flow. *Korea-Aust. Rheol. J.* **2003**, *15* (2), 97–105.
(42) Onogi, S.; Masuda, T.; Matsumoto, T. Nonlinear behavior of viscoelastic materials. I: Disperse systems of polystyrene solution and carbon black. *Trans. Soc. Rheol.* **1970**, *14*, 275–294.
(43) Hatzikiriakos, S. G.; Dealy, J. M. Wall slip of molten high density polyethylene. I. Sliding plate rheometer studies. *J. Rheol.* **1991**, *35* (4), 497–523.
(44) Reimers, M. J.; Dealy, J. M. Sliding plate rheometer studies of concentrated polystyrene solutions: Large amplitude oscillatory shear of a very high molecular weight polymer in diethyl-phthalate. *J. Rheol.* **1996**, *40* (1), 167–186.
(45) Klein, C. O.; Spiess, H. W.; Calin, A.; Balan, C.; Wilhelm, M. Separation of the Nonlinear Oscillatory Response into a Superposition of Linear, Strain Hardening, Strain Softening, and Wall Slip Response. *Macromolecules* **2007**, *40*, 4250–4259.

MA800540N